Available online at www.sciencedirect.com
ScienceDirect
Fluid Phase Equilibria 260 (2007) 36–48
FLUID PHASE EQUILIBRIA
www.elsevier.com/locate/fluid

Experimental densities, vapor pressures, and critical point, and a fundamental equation of state for dimethyl ether

E. Christian Ihmels [a,*], Eric W. Lemmon [b]

[a] *Laboratory for Thermophysical Properties LTP GmbH, Institute at the University of Oldenburg, Marie-Curie-Str. 10, D-26129 Oldenburg, Germany*
[b] *Physical and Chemical Properties Division, National Institute of Standards and Technology, 325 Broadway, Boulder, CO 80305, USA*

Received 31 May 2006; received in revised form 16 September 2006; accepted 18 September 2006
Available online 22 September 2006

This paper is dedicated to the 60th birthday anniversary of Prof. Dr. Jürgen Gmehling.

Abstract

Densities, vapor pressures, and the critical point were measured for dimethyl ether, thus, filling several gaps in the thermodynamic data for this compound. Densities were measured with a computer-controlled high temperature, high-pressure vibrating-tube densimeter system in the sub- and supercritical states. The densities were measured at temperatures from 273 to 523 K and pressures up to 40 MPa (417 data points), for which densities between 62 and 745 kg/m^3 were covered. The uncertainty (where the uncertainties can be considered as estimates of a combined expanded uncertainty with a coverage factor of 2) in density measurement was estimated to be no greater than 0.1% in the liquid and compressed supercritical states. Near the critical temperature and pressure, the uncertainty increases to 1%. Using a variable volume apparatus with a sapphire tube, vapor pressures and critical data were determined. Vapor pressures were measured between 264 and 194 kPa up to near the critical point with an uncertainty of 0.1 kPa. The critical point was determined visually with an uncertainty of 1% for the critical volume, 0.1 K for the critical temperature, and 5 kPa for the critical pressure. The new vapor pressures and compressed liquid densities were correlated with the simple TRIDEN model. The new data along with the available literature data were used to develop a first fundamental Helmholtz energy equation of state for dimethyl ether, valid from 131.65 to 525 K and for pressures up to 40 MPa. The uncertainty in the equation of state for density ranges from 0.1% in the liquid to 1% near the critical point. The uncertainty in calculated heat capacities is 2%, and the uncertainty in vapor pressure is 0.25% at temperatures above 200 K. Although the equation presented here is an interim equation, it represents the best currently available.

Keywords: Critical point; Data; Density; Dimethyl ether; Equation of state; Experimental method; Vapor pressure

1. Introduction

This work is a project between the Laboratory for Thermophysical Properties (LTP) in Oldenburg, Germany, and the National Institute of Standards and Technology (NIST) in Boulder, Colorado to characterize the properties of dimethyl ether. This work on dimethyl ether is a continuation of similar former collaborations on other important compounds such as sulfur dioxide [1] and the butene isomers [2,3].

Dimethyl ether (DME) is an industrially important compound used as a starting material for the production (reaction with sulfur trioxide) of dimethyl sulfate and can be used for large-scale production of acetic acid (reaction with carbon monoxide and water) instead of methanol. It is an excellent methylating agent in the dye industry. Further possible uses of dimethyl ether are the production of olefins, such as ethene, propene, and butenes, using zeolitic catalysts, or saturated hydrocarbons. Dimethyl ether has found commercial use as a refrigerant. It is used as a solvent, an extraction agent, a propellant in aerosols, and a fuel in welding, cutting, and brazing. As a clean-burning synthetic fuel, dimethyl ether can substitute for conventional diesel or liquefied petroleum gas, or be reformed into hydrogen for fuel cells. In contrast to most other aliphatic ethers, dimethyl ether has the advantage that it is not susceptible to autoxidation and is stable with oxygen in air. Furthermore, dimethyl ether is nontoxic and not irritating to skin.

* Corresponding author. Tel.: +49 441 361119 23; fax: +49 441 361119 24.
E-mail address: ihmels@ltp-oldenburg.de (E.C. Ihmels).

0378-3812/$ – see front matter © 2006 Elsevier B.V. All rights reserved.
doi:10.1016/j.fluid.2006.09.016

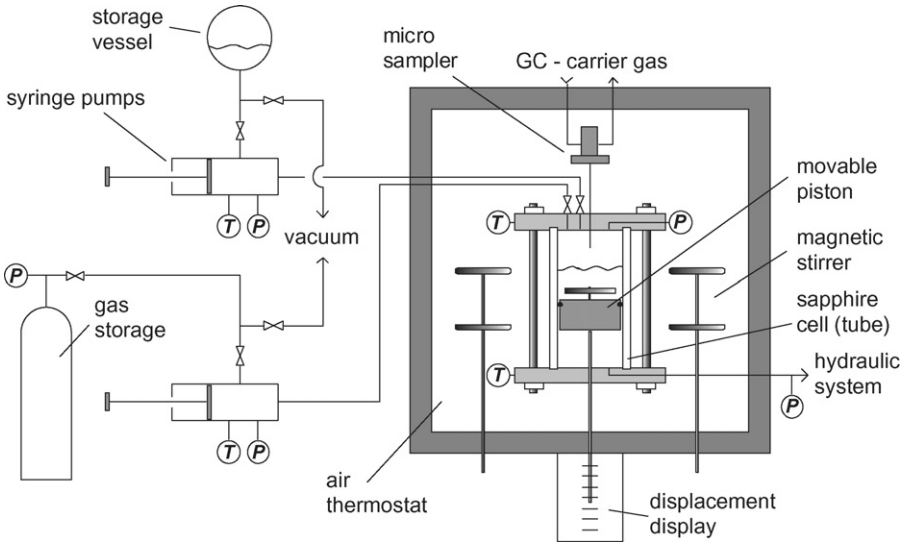

Fig. 1. Schematic diagram of the static apparatus with variable volume.

Many thermodynamic properties are needed for the design of, e.g., industrial plants, pipelines, pumps, or refrigeration cycles. Equations of state are used for the calculation of such properties. In recent years, multiparameter equations of state explicit in the Helmholtz energy have become very common [4]. This type of equation of state allows for the precise calculation of vapor–liquid phase equilibria, $P\rho T$, and other thermodynamic properties such as enthalpies, entropies, heat capacities, and heats of vaporization at given conditions (e.g., temperature, pressure or density). A sufficient amount of reliable thermodynamic data such as vapor pressures, $P\rho T$ data, ideal gas heat capacities, and critical region data are needed for the development of a precise equation. For dimethyl ether, several thermophysical data can be found in the literature. However, they are often of doubtful reliability or inconsistent, or there are problematical gaps in the available data. With the data presented in this paper, we fill some gaps in the $P\rho T$ data surface, extend the available vapor pressures, and report critical point data for dimethyl ether to enable the development of a reliable equation of state for the fluid states. Densities were measured with a vibrating tube densimeter at temperatures from 273 to 523 K at pressures between 0.87 and 40 MPa (417 data points), for which densities between 62 and 745 kg/m^3 were covered. Using a variable volume static apparatus with a sapphire tube, vapor pressures and critical data were determined. Vapor pressures were measured between 264 and 397 K (19 data points). The critical point was visually determined at 400.3 K, 5340.5 kPa, and 277 kg/m^3.

For ease of use, the new vapor pressures and compressed liquid densities were correlated up to 388 K with the TRIDEN model [5]—a combination of the Tait, Rackett, and Wagner equations. Along with the available literature data, the new measured data were used to develop a first comprehensive fundamental equation of state. Because there are still data gaps, further measurements are planned for dimethyl ether to extend the available database and revise this interim equation of state.

2. Experimental measurements

2.1. Sample material

Dimethyl ether (methoxymethane, RE170, C_2H_6O, M = 46.06844 g/mol, CAS-RN 115-10-6) was obtained from Sigma–Aldrich (Germany)[1] and used without any further purification. The purity (better than 99.9 mass%) was checked by gas chromatography both before and after the measurements.

2.2. Variable volume apparatus

The static apparatus shown in Fig. 1 was applied to the measurement of phase equilibrium properties, critical data, and volumetric properties [2]. It can be operated at temperatures between 250 and 440 K and pressures up to 10 MPa. A stirred equilibrium cell consisting of a sapphire tube, which is mounted between two Hastelloy C276 pieces, was placed in an air thermostat (ARMINES, France). Two piston pumps can be used to inject known amounts of the desired components. For the pressure measurement, a calibrated pressure sensor (model PDCR 911, Druck) is connected to the cell. The temperature was measured at the top and bottom of the cell with PT 100 platinum resistance thermometers (ITS-90). The variable volume of the cell is enabled by a hydraulically movable piston, and the change of the position could be observed with the help of a displacement measurement so that volumetric observations could also be made.

The vapor pressures and critical properties measured in this project were determined with this apparatus. Therefore, the volume conditions of the cell were determined. A defined amount

[1] Certain trade names and products are identified only to document the experimental equipment and procedure. This constitutes neither a recommendation or endorsement of these products, nor that the products are necessarily the best available for the purpose.

of substance was injected into the cell, and then the temperature was increased, whereby the phase boundary was kept near the middle of the cell by adjusting the volume of the cell. As the temperature approaches the critical temperature, the change of the phase boundary is very strong and fast. Therefore, the temperature needs to be increased very slowly so that the critical volume can be derived from these measurements. Finally, when the critical point is reached, the disappearance of the phase boundary and the critical opalescence can be observed. The estimated experimental uncertainties for the determination of critical points for pure components with this apparatus are 0.1 K and 5 kPa, and about 1% for the critical volume. Uncertainties of $(0.1 + 0.001P)$ kPa and 0.1 K are estimated for the determination of vapor pressures between 200 and 5200 kPa and temperatures between 265 and 397 K.

2.3. Density apparatus

A computer-operated vibrating-tube densimeter system for high temperatures and pressures (temperatures from 273 to 523 K and pressures up to 40 MPa) was used to measure the density. The automated equipment can be used for the determination of densities in sub-critical and supercritical states. With this apparatus, a large number of data points can be obtained in a rather short time with a minimum of manual effort. A temperature and pressure program can be used to obtain a complete $P\rho T$ field for the desired component. The measurement system was developed in the Ph.D. dissertation of Ihmels [6]. The data for several liquids and liquefied gases (toluene, carbon dioxide, carbonyl sulfide, hydrogen sulfide, sulfur hexafluoride, dinitrogen monoxide, R227ea, and sulfur dioxide) have already been published [5–8]. Comparisons with reference equations of state for toluene, CO_2, and SF_6 demonstrated the high accuracy and suitability of this measurement system for the measurement of fluid densities.

A schematic diagram of the density measurement system is shown in Fig. 2. The apparatus and procedure of the measurements were described in detail by Ihmels and Gmehling [5,7]. A prototype of a high-pressure high-temperature vibrating-tube densimeter (DMA-HDT, Hastelloy C-276, Stabinger, Austria) is the essential part of the experimental setup. The temperature was measured with a Pt100 resistance thermometer (ITS-90), and the pressure was monitored by means of a calibrated external pressure sensor (Model PDCR 911, pressure range 60 MPa). The density values were obtained from the periods of oscillation of the vibrating tube.

2.4. Calibration, accuracy, and precision of measured values

For the calibration of the density measurement apparatus, the period of oscillation at zero pressure (between 273 and 523 K) and for the two reference substances, water (between 278 and 523 K and up to 40 MPa) and butane (273 and 425 K and up to 40 MPa) in the compressed liquid, were used. The reference densities were calculated from the reference equations of state from Wagner and Pruß [9] for water and from Younglove and Ely [10] for butane. The uncertainty in temperature measurements is estimated to be 0.03 K, and the measurement of pressure has an estimated uncertainty of 6 kPa (calibrated with a dead weight balance). The density measurements in the temperature, pressure, and density range covered with the calibration (273–523 K, 0.9–35 MPa, 500–1000 kg/m^3) have an uncertainty of 0.2 kg/m^3 for liquid densities. For the liquid densities measured in this work between 400 and 745 kg/m^3 and the compressed supercritical densities between 300 and 600 kg/m^3, a maximum uncertainty of 0.1% was estimated taking into account the influence of the calibration EOS and the influence of temperature, pressure, and period of oscillation dependencies. Because of the strong pressure dependence of the densities near the critical point, higher deviations were obtained in this region. With an uncertainty of 6 kPa, a maximum error in density of about 1% in the region near the critical point and in the supercritical region ($T > T_c$) near the critical pressure is estimated.

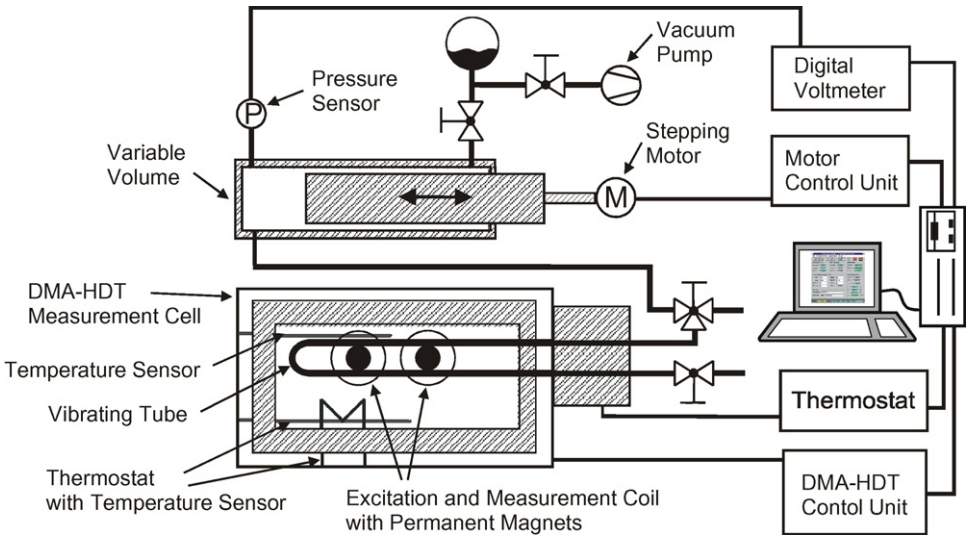

Fig. 2. Schematic diagram of the computer-controlled density measurement unit.

3. Experimental results

3.1. Vapor pressures and critical data

The vapor pressures of dimethyl ether were measured between 264 and 397 K. The experimental results of the vapor pressure measurements are listed in Table 1. The critical point was determined as 400.3 K, 5340.5 kPa, and 277 kg/m^3. With the new critical data, the experimental vapor pressures were correlated with the Wagner equation in the "2.5.5" form [11],

$$\ln\left(\frac{P}{P_c}\right) = \frac{A_W(1-T_r) + B_W(1-T_r)^{1.5} + C_W(1-T_r)^{2.5} + D_W(1-T_r)^5}{T_r}, \quad (1)$$

where T_r is T/T_c. The parameters are given in Table 2. Comparisons with the experimental values, the Wagner correlation given in this equation, and values taken from the literature are presented later. The average absolute deviation between the vapor pressures and calculations with the Wagner equation is 0.04% for the new experimental vapor pressures. The measured critical volume of 277 kg/m^3 lies between the literature values of 272 kg/m^3 [12] and 280 kg/m^3 [13].

Table 1
Experimental vapor pressures for dimethyl ether

T (K)	P (kPa)
264.30	193.5
274.63	281.6
280.50	342.4
290.14	465.4
295.12	540.1
307.86	773.2
312.92	880.9
326.76	1245.9
327.44	1267.1
333.81	1467.9
334.79	1504.9
340.67	1712.0
354.66	2297.8
361.18	2620.5
376.03	3463.4
383.17	3950.7
390.42	4486.5
394.44	4812.1
397.46	5083.6

Table 2
Parameters of the Wagner vapor pressure equation for dimethyl ether

A_W	−7.19
B_W	2.148
C_W	−2.452
D_W	−1.906
P_c (kPa)	5340.5
T_c (K)	400.3
T_{min} (K)	200
T_{max} (K)	400.3
AAD (%)	0.10

3.2. PρT results

The densities of dimethyl ether were measured from 273 to 523 K and from 0.9 to 40 MPa. The experimental results (417 data points) are listed in Table 3 and presented graphically in Fig. 3. The measured compressed liquid densities between 273 and 388 K were correlated with the three-dimensional $P\rho T$-correlating model TRIDEN [5,6]. In this model the Tait equation [14] for isothermal compressed densities was combined with a modified Rackett equation [15] for the liquid saturation densities and the Wagner vapor pressure equation [11] in the "2.5.5" form. The liquid saturation density and the vapor pressure are used as a reference state (ρ_0 and P_0) for the Tait equation. With these equations, it is possible to correlate the $P\rho T$ data over the whole liquid state up to nearly the critical point within the experimental uncertainties.

For temperatures below the normal boiling point, the reference pressure was set to $P_0 = 0.1013$ MPa. The reference densities ρ_0 at P_0 (saturation pressure or 0.1013 MPa) were extrapolated from the compressed liquid density measurements and correlated with the modified Rackett equation:

$$\rho_0 = \frac{A_R}{B_R^{[1+(1-T/C_R)^{D_R}]}}. \quad (2)$$

For the Tait equation,

$$\rho = \frac{\rho_0}{[1 - C_T \ln((B_T + P)/(B_T + P_0))]}, \quad (3)$$

where the following temperature dependence was used for the parameter B_T:

$$B_T = B_{T_0} + B_{T_1}\frac{T}{E_T} + B_{T_2}\left(\frac{T}{E_T}\right)^2 \quad (4)$$

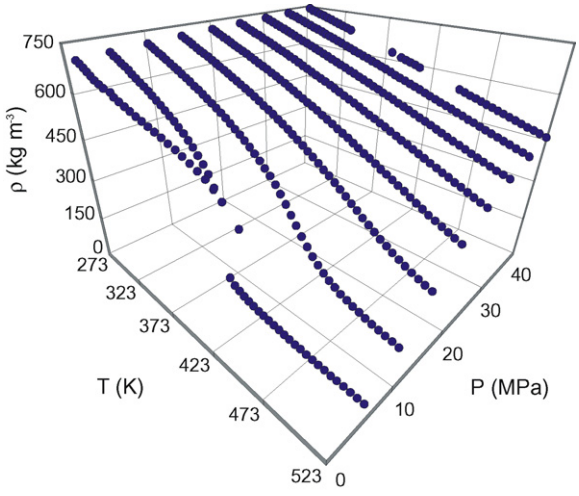

Fig. 3. Experimental densities for dimethyl ether.

Table 3
Experimental densities of dimethyl ether

T (K)	P (MPa)	ρ (kg/m^3)
273.22	0.877	700.79
273.23	4.990	706.75
273.23	9.990	713.44
273.23	15.009	719.62
273.23	20.004	725.34
273.23	25.005	730.68
273.23	29.992	735.71
273.23	34.995	740.46
273.23	40.004	744.95
278.23	0.880	693.36
278.24	4.998	699.68
278.23	9.991	706.71
278.23	14.995	713.18
278.23	19.994	719.15
278.23	25.006	724.73
278.23	29.989	729.93
278.23	34.996	734.86
278.24	39.991	739.50
283.24	0.910	685.80
283.25	4.995	692.46
283.25	9.986	699.88
283.25	14.999	706.67
283.25	19.995	712.92
283.25	24.987	718.70
283.25	29.992	724.13
283.25	35.004	729.24
283.25	39.989	734.06
288.25	0.909	678.03
288.26	4.982	685.10
288.26	10.010	693.00
288.26	14.994	700.10
288.26	19.986	706.62
288.26	24.993	712.67
288.26	29.993	718.31
288.26	34.996	723.60
288.26	39.987	728.59
293.27	0.909	670.08
293.27	4.998	677.66
293.27	9.998	685.98
293.27	14.994	693.46
293.27	19.996	700.29
293.27	24.988	706.60
293.27	29.991	712.46
293.27	35.000	717.94
293.27	40.002	723.12
298.28	0.906	661.92
298.28	4.995	670.04
298.28	9.992	678.86
298.28	14.993	686.76
298.28	19.995	693.93
298.28	25.012	700.51
298.28	30.006	706.62
298.28	35.002	712.29
298.28	40.007	717.61
303.29	1.000	653.78
303.30	4.987	662.26
303.30	10.002	671.67
303.30	14.991	679.99
303.30	19.989	687.50
303.30	24.998	694.37
303.30	29.999	700.74
303.30	34.991	706.62
303.30	40.004	712.17
308.31	1.105	645.43

Table 3 (*Continued*)

T (K)	P (MPa)	ρ (kg/m^3)
308.31	4.991	654.33
308.31	10.014	664.37
308.31	15.004	673.15
308.31	20.005	681.03
308.31	25.005	688.23
308.31	29.992	694.81
308.31	35.001	700.95
308.31	40.012	706.66
313.21	1.397	637.53
313.21	4.989	646.35
313.21	9.994	657.00
313.21	15.001	666.32
313.21	19.997	674.60
313.21	24.995	682.09
313.21	29.991	688.96
313.21	34.992	695.31
313.21	40.004	701.22
318.22	1.345	628.29
318.22	4.991	638.01
318.22	9.986	649.41
318.22	15.015	659.30
318.22	20.005	668.00
318.22	24.987	675.80
318.22	30.001	682.98
318.22	35.007	689.57
318.22	39.994	695.71
323.22	1.480	619.24
323.23	4.996	629.43
323.23	9.988	641.66
323.23	14.994	652.11
323.23	19.984	661.28
323.23	24.989	669.49
323.23	29.986	676.94
323.23	34.997	683.81
323.22	39.986	690.14
328.23	1.626	609.90
328.23	4.983	620.53
328.23	9.993	633.76
328.23	15.000	644.87
328.23	20.005	654.54
328.23	24.992	663.11
328.23	29.999	670.92
328.23	35.001	678.03
328.23	39.997	684.60
333.23	1.756	600.12
333.23	4.989	611.37
333.24	9.997	625.66
333.23	14.998	637.49
333.23	19.985	647.66
333.23	25.003	656.72
333.23	30.007	664.81
333.23	35.006	672.22
338.23	1.958	590.18
338.24	4.998	601.88
338.24	10.012	617.39
338.24	15.003	629.99
338.24	19.984	640.73
338.24	24.986	650.20
338.24	30.004	658.70
338.24	34.991	666.37
343.24	2.158	579.80
343.24	4.991	591.92
343.24	9.998	608.84
343.24	15.006	622.36
343.24	20.006	633.76

Table 3 (*Continued*)

T (K)	P (MPa)	ρ (kg/m^3)
343.24	25.003	643.68
343.24	29.996	652.52
343.24	35.006	660.51
348.24	2.331	568.71
348.24	4.984	581.48
348.25	9.985	600.02
348.24	14.988	614.53
348.25	19.993	626.62
348.25	25.000	637.06
348.25	30.002	646.30
348.25	34.994	654.61
353.24	2.571	557.37
353.25	4.990	570.54
353.25	9.991	591.00
353.25	14.989	606.58
353.25	20.004	619.43
353.25	24.985	630.35
353.25	30.003	640.04
353.25	35.012	648.69
358.25	2.813	545.31
358.25	4.988	558.91
358.25	9.992	581.65
358.25	15.001	598.50
358.25	20.005	612.10
358.25	25.002	623.64
358.25	29.996	633.72
358.25	34.991	642.71
363.25	3.057	532.40
363.25	4.999	546.53
363.26	9.999	572.01
363.26	14.993	590.17
363.25	20.013	604.70
363.25	25.006	616.81
363.26	29.996	627.36
363.25	35.003	636.74
368.26	3.329	518.62
368.26	4.993	533.02
368.26	10.002	561.96
368.26	14.990	581.67
368.26	20.010	597.14
368.26	24.993	609.90
368.26	29.996	620.95
368.26	34.994	630.70
373.26	3.610	503.51
373.26	4.992	518.21
373.26	9.993	551.46
373.26	14.987	572.95
373.26	20.012	589.46
373.26	24.996	602.93
373.26	29.991	614.48
373.26	34.996	624.65
378.26	3.908	486.95
378.26	4.988	501.49
378.27	10.000	540.53
378.27	15.005	564.09
378.26	19.995	581.63
378.26	24.996	595.88
378.26	29.996	607.99
378.26	35.015	618.53
378.26	40.001	627.97
383.26	4.228	468.41
383.26	4.995	482.23
383.27	10.006	529.06
383.27	14.994	554.89
383.26	19.997	573.70

Table 3 (*Continued*)

T (K)	P (MPa)	ρ (kg/m^3)
383.26	24.996	588.78
383.26	29.990	601.42
383.26	34.995	612.43
388.26	4.559	446.74
388.26	4.995	458.35
388.27	9.998	516.89
388.27	14.993	545.44
388.27	19.989	565.63
388.27	25.000	581.57
388.27	29.995	594.82
388.26	34.985	606.25
388.26	40.008	616.40
393.26	4.913	420.40
393.26	4.993	424.35
393.27	9.986	504.06
393.27	14.997	535.78
393.27	19.989	557.39
393.27	24.988	574.20
393.27	29.995	588.14
393.27	35.000	600.05
393.27	39.978	610.56
398.24	5.281	385.81
398.27	9.999	490.42
398.27	14.999	525.78
398.27	19.997	549.06
398.27	24.998	566.84
398.27	29.989	581.38
398.27	34.998	593.82
398.27	39.990	604.68
403.27	5.018	137.43
403.28	9.997	476.07
403.27	15.004	515.69
403.27	19.984	540.57
403.27	25.005	559.42
403.27	30.000	574.63
403.27	34.993	587.51
403.27	40.005	598.79
408.27	5.018	121.72
408.19	6.071	306.98
408.28	9.993	459.93
408.27	14.983	504.92
408.28	20.010	532.09
408.27	25.009	552.00
408.28	29.991	567.91
408.28	34.992	581.38
408.27	39.979	593.07
413.28	5.019	113.40
413.28	9.992	442.27
413.28	15.007	493.84
413.28	20.006	523.02
413.28	25.009	544.18
413.28	29.996	560.89
413.28	35.002	574.91
418.28	5.019	106.83
418.28	10.000	423.38
418.28	14.991	482.36
418.28	19.997	514.01
418.28	25.007	536.40
418.28	30.000	554.01
418.28	35.001	568.61
423.28	5.018	101.50
423.28	9.987	402.16
423.28	15.000	470.72
423.28	19.989	504.83
423.28	24.993	528.60

Table 3 (*Continued*)

T (K)	P (MPa)	ρ (kg/m^3)
423.28	29.999	547.07
423.28	34.987	562.23
428.28	5.016	97.00
428.28	9.992	379.30
428.28	15.005	458.33
428.28	19.992	495.56
428.28	24.999	520.76
428.28	29.999	540.10
428.28	35.007	555.90
433.28	5.013	93.12
433.29	9.988	354.32
433.29	14.989	445.70
433.29	20.001	486.18
433.29	25.001	512.86
433.29	29.994	533.08
433.29	34.994	549.54
438.29	5.012	89.79
438.29	9.994	328.67
438.29	14.983	432.73
438.29	19.989	476.53
438.29	24.989	504.81
438.29	29.998	526.05
438.29	34.984	543.12
443.28	5.015	86.95
443.29	9.989	302.97
443.29	14.992	419.57
443.29	19.991	466.84
443.29	24.983	496.70
443.29	29.994	518.95
443.29	34.983	536.69
448.29	5.015	84.36
448.29	9.994	279.70
448.29	15.005	406.20
448.29	20.009	457.16
448.29	24.990	488.60
448.29	29.997	511.82
448.29	34.993	530.23
448.29	39.997	545.66
453.29	5.019	82.06
453.29	9.992	258.86
453.29	14.991	392.27
453.29	20.007	447.34
453.29	24.990	480.43
453.29	29.992	504.67
453.29	34.994	523.84
453.29	39.989	539.76
458.29	5.019	79.90
458.29	9.989	241.02
458.29	14.984	378.31
458.29	19.995	436.80
458.29	25.014	472.28
458.29	29.998	497.54
458.29	34.987	517.38
458.29	39.998	533.83
463.29	5.018	77.86
463.29	9.991	225.94
463.29	15.002	364.83
463.29	19.996	426.86
463.29	25.009	464.08
463.29	29.990	490.33
463.29	34.992	510.93
463.29	40.009	527.91
468.29	5.016	75.97
468.29	9.983	212.83
468.30	14.995	351.07

Table 3 (*Continued*)

T (K)	P (MPa)	ρ (kg/m^3)
468.29	19.984	416.67
468.29	25.012	455.83
468.29	29.988	483.15
468.29	34.990	504.51
468.29	39.997	522.01
473.29	5.015	74.24
473.29	9.991	202.05
473.30	15.001	337.83
473.29	20.000	406.74
473.29	25.010	447.57
473.29	29.993	476.02
473.29	34.983	498.05
473.29	39.982	516.11
478.29	5.019	72.69
478.30	9.989	192.49
478.30	14.995	324.82
478.30	20.005	396.77
478.30	25.004	439.28
478.30	29.997	468.88
478.30	34.990	491.65
478.30	40.007	510.20
483.29	5.014	71.08
483.30	9.997	184.48
483.29	14.993	312.38
483.29	19.999	386.72
483.30	25.010	431.13
483.29	29.996	461.73
483.29	34.989	485.24
483.29	39.989	504.33
488.29	5.018	69.74
488.29	9.996	177.16
488.30	15.003	300.80
488.30	20.006	376.95
488.29	25.009	422.98
488.29	29.989	454.58
488.29	34.985	478.85
488.30	39.998	498.48
493.29	5.015	68.33
493.29	9.990	170.57
493.30	14.991	289.51
493.29	19.982	367.00
493.30	24.987	414.83
493.30	29.989	447.48
493.29	35.002	472.46
493.29	40.002	492.65
498.29	5.014	67.02
498.29	9.990	164.73
498.30	14.995	279.16
498.30	19.987	357.56
498.30	24.994	406.26
498.29	29.990	440.45
498.29	34.987	466.18
498.30	39.988	486.84
503.29	5.017	65.83
503.29	9.984	159.37
503.30	14.998	269.50
503.29	19.995	348.45
503.29	24.986	398.39
503.29	29.997	433.53
503.29	34.985	459.88
503.29	39.990	481.11
508.29	5.017	64.68
508.29	10.000	154.87
508.29	14.991	260.28
508.29	20.003	339.57

Table 3 (*Continued*)

T (K)	P (MPa)	ρ (kg/m^3)
508.29	24.989	390.63
508.29	29.992	426.58
508.29	34.993	453.66
508.29	39.984	475.38
513.29	5.017	63.54
513.29	9.999	150.52
513.29	14.983	251.73
513.29	20.009	330.95
513.29	25.007	383.08
513.29	29.991	419.74
513.29	34.991	447.49
513.29	39.992	469.70
518.29	5.018	62.50
518.29	10.005	146.60
518.29	14.984	243.95
518.29	20.002	322.53
518.29	24.988	375.36
518.29	29.992	413.00
518.29	34.986	441.33
518.29	39.985	464.06
523.29	5.018	61.47
523.29	9.992	142.61
523.29	14.998	236.92
523.29	19.987	314.25
523.29	24.996	368.03
523.29	29.997	406.36
523.29	34.990	435.28
523.29	39.984	458.46

The TRIDEN parameters for the Tait equation, the Rackett equation, the temperature and pressure ranges covered, and the average absolute deviation (AAD),

$$\mathrm{AAD} = \frac{1}{n}\sum_{n}\left|\frac{\rho_{\mathrm{exp}} - \rho_{\mathrm{calc}}}{\rho_{\mathrm{exp}}}\right|, \tag{5}$$

are given in Table 4. The absolute deviations are usually lower than 0.1% except at the highest temperatures. Until now, only limited literature density data for dimethyl ether are available. Compressed liquid densities have recently been published by Bobbo et al. [16] for the range between 283 and 353 K and up to 35 MPa. These data are in good agreement with the correlation, with an average absolute deviation of 0.07% in density. Comparisons were also made between the TRIDEN correlation and the saturated liquid densities published by different researchers and stored in the Dortmund data bank [17]. The average absolute deviation between the literature values for saturated liquid densities and calculations with the Rackett equation (TRIDEN extrapolation to the saturation pressure) is 0.20% in density for all data available in the range between 273 and 388 K. The densities published by Pall and Maass [18] (between 280 and 388 K, AAD: 0.29%) and Wu et al. [12] (302–384 K, 0.16%) as well as data at lower temperatures from Wu et al. [19] (between 231 and 368 K, AAD: 0.12%), Maass and Boomer [20] (233 and 262 K, 0.15%), and from Calado et al. [21] (at 182 K, 0.84%) are represented well (for all data AAD: 0.18%) by the Rackett equation. This also indicates that the extrapolation behavior is reliable at lower temperatures due to the simplicity of the TRIDEN correlation.

Table 4
Parameters of the TRIDEN correlation for the Tait- and Rackett-equations

T_{min} (K)	273.2
T_{max} (K)	388.3
P_{min} (MPa)	0.88
P_{max} (MPa)	40
ρ_{min} (kg/m^3)	446.7
ρ_{max} (kg/m^3)	745.0
Data points	206
C_{T}	0.0834042
B_{T0}	284.304
B_{T1}	−130.021
B_{T2}	14.4194
E_{T}	100
A_{R}	55.6001
B_{R}	0.236704
C_{R}	401.406
D_{R}	0.243368
AAD (%)	0.039

4. Fundamental equation of state

A 10-parameter equation of state for dimethyl ether was fitted with the Helmholtz energy as the fundamental property with independent variables of density and temperature. For its development, the measured densities plus additional $P\rho T$ data, vapor pressures, critical data, ideal gas heat capacities, and isobaric heat capacities from the TRC [22,23] and Dortmund [17] databanks were used. The equation of state is valid from 131.65 K (the triple point temperature) to 525 K and for pressures up to 40 MPa.

5. Fitting of the equation of state

5.1. Form of the equation of state

The interim equation of state presented here for dimethyl ether was formulated with the Helmholtz energy as the fundamental property [3,4] with independent variables of density and temperature. The equation of state is given by

$$a(\rho, T) = a^0(\rho, T) + a^{\mathrm{r}}(\rho, T), \tag{6}$$

where a is the Helmholtz energy, $a^0(\rho,T)$ is the ideal gas contribution to the Helmholtz energy, and $a^{\mathrm{r}}(\rho,T)$ is the residual Helmholtz energy. All thermodynamic properties can be calculated as derivatives of the Helmholtz energy. The functional form is explicit in the dimensionless Helmholtz energy, α, using independent variables of dimensionless density and temperature. The form of this equation is

$$\frac{a(\rho, T)}{RT} = \alpha(\delta, \tau) = \alpha^0(\delta, \tau) + \alpha^r(\delta, \tau) \tag{7}$$

where $\delta = \rho/\rho_{\mathrm{c}}$, $\tau = T_{\mathrm{c}}/T$, the critical temperature (T_{c}) is 400.3 K (ITS-90), and the critical density (ρ_{c}) is 6.013 mol/dm^3 ($\approx$277 kg/m^3). The critical pressure, P_{c}, is 5340.5 kPa. These critical values are those reported earlier in this work. The ideal

gas Helmholtz energy is given in a dimensionless form by

$$\alpha^0 = \frac{h_0^0\tau}{RT_c} - \frac{s_0^0}{R} - 1 + \ln\frac{\delta\tau_0}{\delta_0\tau} - \frac{\tau}{R}\int_{\tau_0}^{\tau}\frac{c_p^0}{\tau^2}\,d\tau + \frac{1}{R}\int_{\tau_0}^{\tau}\frac{c_p^0}{\tau}\,d\tau, \quad (8)$$

where $\delta_0 = \rho_0/\rho_c$, $\tau_0 = T_c/T_0$, and T_0, ρ_0, h_0^0, and s_0^0 are used to define an arbitrary reference state point. The equation (developed here) for the ideal gas heat capacity is given by

$$\frac{c_p^0}{R} = 4.039 + \sum_{i=1}^{4} v_i\left(\frac{u_i}{T}\right)^2\frac{\exp(u_i/T)}{[\exp(u_i/T)-1]^2}, \quad (9)$$

where $u_1 = 361$ K, $u_2 = 974$ K, $u_3 = 1916$ K, $u_4 = 4150$ K, $v_1 = 2.641$, $v_2 = 2.123$, $v_3 = 8.992$, $v_4 = 6.191$, and the universal gas constant, R, is 8.314472 J/(mol K). This equation is valid from 100 K to the dissociation limit of dimethyl ether. A more convenient form of the ideal gas Helmholtz energy, derived from the integration of Eq. (8) and the application of a reference state with zero enthalpy and entropy at the normal boiling point for the saturated liquid, is

$$\alpha^0 = \ln\delta + 3.039\ln\tau + a_1 + a_2\tau + \sum_{i=1}^{4} v_i \ln\left[1 - \exp\left(\frac{-u_i\tau}{T_c}\right)\right] \quad (10)$$

where $a_1 = -1.928925$ and $a_2 = 3.150284$. The functional form for the residual Helmholtz energy is

$$\alpha^r(\delta,\tau) = \sum_{k=1}^{4} N_k\delta^{i_k}\tau^{j_k} + \sum_{k=5}^{10} N_k\delta^{i_k}\tau^{j_k}\exp(-\delta^{l_k}), \quad (11)$$

where the coefficients and exponents determined in this work are given in Table 5. The equations used to calculate pressure, enthalpy, heat capacity, speed of sound, etc., from the equation of state are given by Span and Wagner [24]. The equation of state is valid from 131.65 to 525 K with pressures up to 40 MPa. The uncertainty (where the uncertainties can be considered as estimates of a combined expanded uncertainty with a coverage factor of 2) in density of the equation of state ranges from 0.1% in the liquid to 1% near the critical point. The uncertainty in heat capacities is 2%, and the uncertainty in vapor pressure is 0.25% at temperatures above 200 K. In the critical region, the uncertainties are higher for all properties except vapor pressure.

Table 5
Coefficients and exponents of the equation of state

k	N_k	i_k	j_k	l_k
1	1.22690	0.21	1	0
2	−2.47245	1.0	1	0
3	0.119889	0.5	3	0
4	0.0000354	1.0	8	0
5	0.567139	1.4	2	1
6	0.166649	3.1	1	1
7	−0.078412	1.5	5	1
8	−0.289066	5.0	1	2
9	−0.031272	5.9	4	2
10	−0.065607	3.7	3	2

5.2. Data used in the fit

The data used in the fitting and evaluation of the equation of state are listed in Table 6 along with the absolute average deviations of values calculated from the data and the equation of state. An initial equation was developed by nonlinearly fitting a small subset of the available data ($P\rho T$, vapor pressures, etc.) to the functional form given by Span and Wagner [24]. From this preliminary equation, the exponents of the equation were allowed to float, similar to the method used in the work of Lemmon et al. [25]. The $P\rho T$ data used in the fit comprise the data measured in this work and some of the data of Bobbo et al. [16]. In addition, the vapor pressure data reported here, and some of the data of Bobbo et al. [26–30] and Kennedy et al. [43] were used in the fitting process. In the critical region, the saturated liquid and vapor phase densities of Wu et al. [12,19] were used to model the critical region. The isobaric heat capacities of Kennedy et al. for the saturated liquid phase were used to control the caloric properties at low temperatures. The critical point of the equation of state (the point at which $dP/d\rho$ and $d^2P/d\rho^2$ are simultaneously equal to zero) was constrained to the selected critical point values given earlier.

5.3. Comparisons with the data

The calculated ideal gas heat capacities of Chao and Hall [34] are represented by Eq. (9) to within ±0.01% up to 2500 K. Higher deviations are obtained for the other data sets, with deviations of up to 0.8% for the data of Seha [50] and of Kistiakowsky and Rice [44], and with deviations of 1–1.7% for

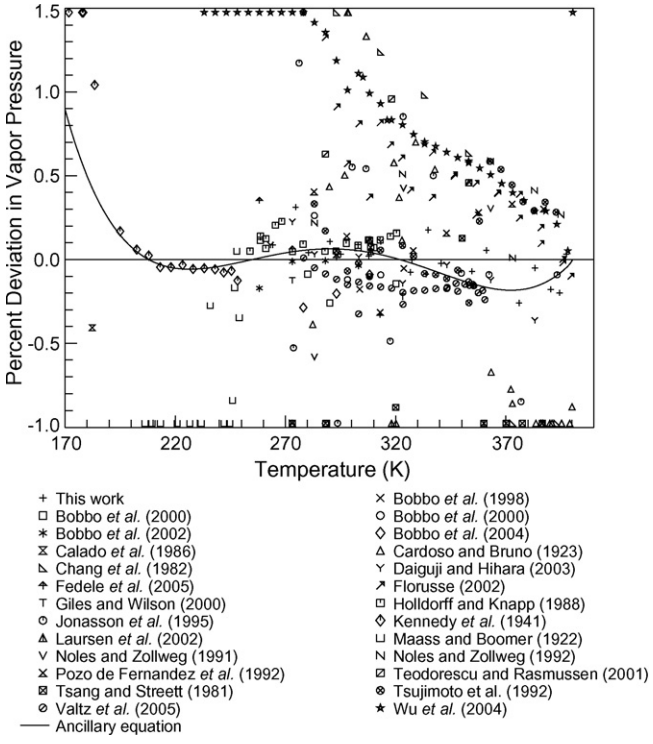

Fig. 4. Comparisons of vapor pressures calculated with the equation of state to experimental data.

Table 6
Experimental data for dimethyl ether

Author	No. of points	Temperature range (K)	Pressure range (MPa)	AAD[a] (%)
$P\rho T$				
Bobbo et al. [16]	96	283–353	0.55–35.5	0.053
This work	417	273–523	0.877–40	0.083
Vapor pressure				
Bobbo et al. [26]	2	304–324	0.688–1.16	0.12
Bobbo et al. [27]	4	280–320	0.338–1.06	0.14
Bobbo et al. [28]	3	283–313	0.374–0.89	0.16
Bobbo et al. [29]	4	258–303	0.152–0.679	0.06
Bobbo et al. [30]	3	278–308	0.316–0.778	0.19
Calado et al. [21]	1	182	0.002	0.41
Cardoso and Bruno [31]	23	273–400	0.255–5.27	1.08
Chang et al. [33]	7	273–393	0.255–4.66	1.68
Daiguji and Hihara [35]	10	263–383	0.186–3.94	0.12
Fedele et al. [37]	3	258–293	0.153–0.509	0.14
Florusse et al. [38]	24	288–399	0.442–5.26	0.46
Giles and Wilson [39]	2	273–323	0.266–1.14	0.17
Holldorff and Knapp [41]	19	254–320	0.128–1.07	0.11
Jonasson et al. [42]	14	274–393	0.27–4.72	0.93
Kennedy et al. [43]	16	172–248	0.001–0.101	1.22
Laursen et al. [45]	5	298–320	0.6–1.03	1.19
Maass and Boomer [20]	13	206–249	0.01–0.104	2.21
Noles and Zollweg [47]	3	283–363	0.371–2.73	0.44
Noles and Zollweg [48]	6	283–395	0.374–4.88	0.33
Pozo de Fernandez et al. [49]	8	283–387	0.372–4.26	0.25
Teodorescu and Rasmussen [51]	4	288–353	0.44–2.24	0.54
Tsang and Streett [52]	9	273–387	0.26–4.11	1.50
Tsujimoto et al. [53]	22	283–393	0.374–4.7	0.21
Valtz et al. [54]	27	278–361	0.318–2.58	0.16
Wu et al. [55]	39	233–400	0.055–5.36	1.65
This work	19	264–397	0.194–5.08	0.11
Saturated liquid density				
Bobbo et al. [16]	7	283–343		0.11
Calado et al. [21]	1	182		0.11
Cardoso and Coppola [32]	12	273–400		1.31
Grosse et al. [40]	9	193–273		0.40
Maass and Boomer [20]	11	233–262		0.13
Pall and Maass [18]	26	281–393		0.30
Wu et al. [12]	18	302–400		0.65
Wu et al. [19]	31	213–368		0.11
Saturated vapor density				
Cardoso and Coppola [32]	12	273–400		6.6
Kennedy et al. [43]	1	246		14
Wu et al. [12]	7	367–400		7.4
Wu et al. [19]	31	213–368		2.9
Ideal gas isobaric heat capacity				
Chao and Hall [34]	25	50–3000		0.005
Eucken and Frank [36]	2	200–280		1.19
Kistiakowsky and Rice [44]	4	272–370		0.55
Miyazaki [46]	3	303–343		1.39
Seha [50]	9	298–1000		0.40
Isobaric heat capacity				
Kennedy et al. [43]	32	129–246	Saturated liquid	1.4
Kistiakowsky and Rice [44]	4	272–370	0.1–0.101	5.2
Miyazaki [46]	12	303–343	0.2–0.5	4.1

[a] Absolute average deviation in the specified property.

the data of Miyazaki [46]. The equation represents the saturated liquid isobaric heat capacity data of Kennedy et al. [43] within 0.5%, except for the two highest temperatures near 240 K, where the deviations are 0.8%. Comparisons of experimental vapor pressures with values calculated from the equation of state by applying the phase equilibrium condition are presented in Fig. 4 as $100 \times (P_{exp} - P_{calc})/P_{exp}$. There are considerable differences and scatter between the various data sets for vapor pressure. These data appear to be grouped into three separate sets. The grouping used in fitting the equation of state shows random scatter about the equation of state with deviations of up to 0.25%. These measurements are available from 250 K to the critical point, with one data set that extends down to 200 K (that of Kennedy et al.) The second grouping is somewhat consistent with the first grouping near the critical point, but increases to 1% at about 280 K. The third grouping shows deviations below the equation of 1–2%. Data sets within the first grouping include those measured in this work, and the measurements of Bobbo et al. [26–30], Daiguji and Hihara [35], Holldorff and Knapp [41], and Valtz et al. [54].

In the compressed liquid (subcritical and supercritical), densities of dimethyl ether have previously been measured from 283 to 353 K with pressures up to 36 MPa by Bobbo et al. [16]. They also reported saturated densities in the liquid phase. With the new measurements presented here, compressed liquid densities are now available down to 273 K and up to 523 K. Below 273 K, only saturated liquid densities are available to evaluate density deviations of the equation of state for DME. These include the data of Calado et al. [21], Grosse et al. [40], Maass and Boomer [20], and Wu et al. [19].

Deviations between the experimental $P\rho T$ data and the equation of state are shown in Fig. 5 as $100 \times (\rho_{exp} - \rho_{calc})/\rho_{exp}$. All of the densities measured in this work and those of Bobbo et al. [16] are represented with an average absolute deviation of 0.08%. The data presented here at temperatures below 390 K have an average absolute deviation of 0.02%. Saturated liquid densities below 370 K are generally represented within 0.2% in

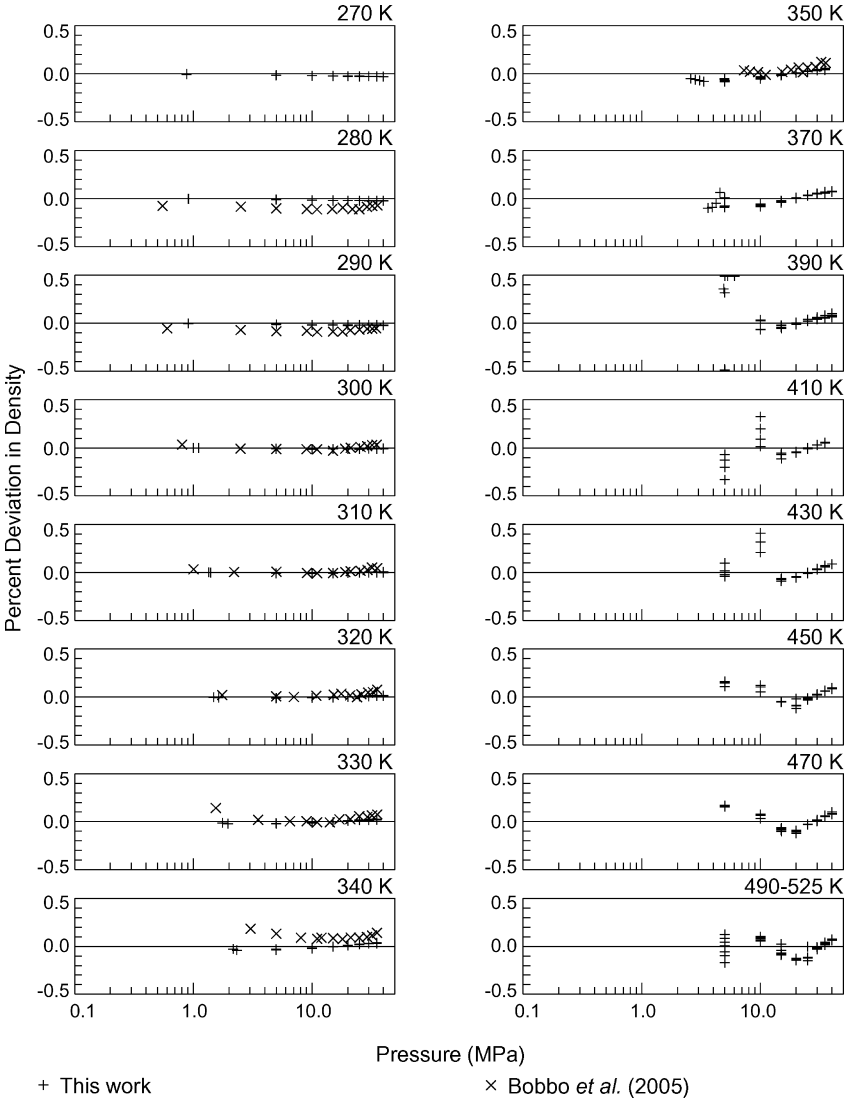

Fig. 5. Comparisons of densities calculated with the equation of state to experimental data.

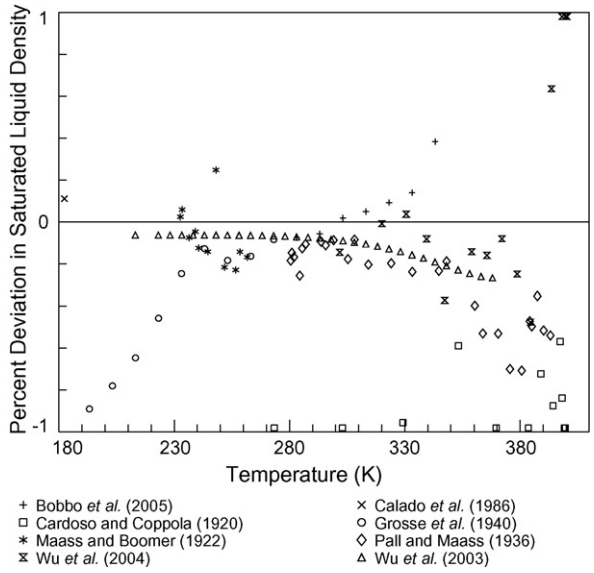

Fig. 6. Comparisons of saturated liquid densities calculated with the equation of state to experimental data.

density except for the data of Grosse et al. [40]. One data point by Calado et al. [21] was measured at 182 K and the equation deviates from this point by 0.11%. Aside from the data of Grosse et al., the next data set with the lowest temperature is that by Wu et al. [19] at a temperature of 213 K. The equation represents their lowest temperature data point by −0.06% and their highest temperature point by −0.27% (at 368 K). The higher deviation at 368 K is caused by inconsistencies between the data measured here in the single phase and those of Wu et al. The data of Bobbo et al. [16] also show opposite trends from the data of Wu et al. with positive deviations from the equation. The equation deviates from the saturated vapor densities (the only density measurements in the vapor phase) by up to 5% above 300 K for the four available sets. The scatter between these sets is quite

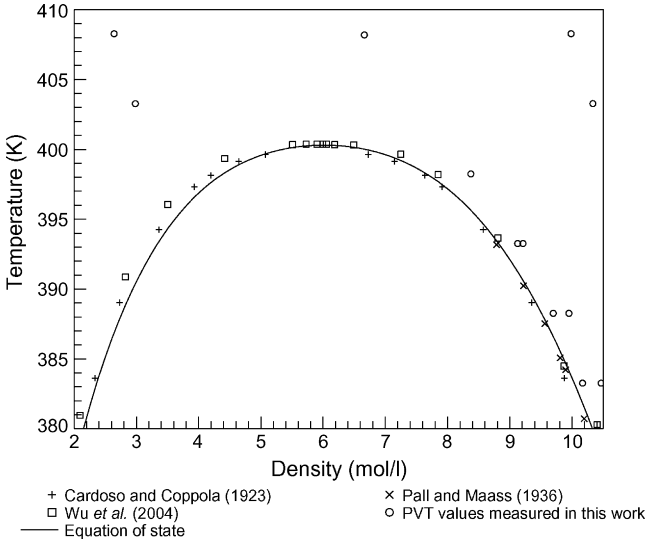

Fig. 7. Critical region saturated densities taken from the literature and pressure–temperature–density measurements presented in this work.

large (resulting in the 5% deviations), and additional vapor phase measurements are needed to clarify the vapor phase situation. Fig. 6 shows comparisons between saturated liquid calculations from the equation of state with the available experimental data. Fig. 7 shows how the critical region saturation data overlap the calculated values. The single-phase $P\rho T$ data measured in this work in the critical region are also shown in this figure, indicating the need for additional measurements.

In the development of equations of state, various data types are useful in evaluating other types of data. Since one equation is used to represent multiple properties, the accuracy of one property can influence the behavior of another. In particular, the availability of heat capacity data is fundamental in the development of the equation of state. Without it, equations can inadvertently give negative heat capacities at low temperatures or show unrealistic curvature in certain areas of the fluid surface. Although the amount of heat capacity data for DME is limited, it does cover the saturated liquid range, and comparisons with the equation are favorable. In addition, the functional form of the equation of state is limited to only 10 coefficients (as compared with 20–50 terms in high accuracy equations). The limited number of coefficients increases the ability of the equation to accurately give proper values of derived properties of a fluid based upon limited experimental data. Such behavior is confirmed by plotting various constant property lines over the surface of state, and by comparing the slopes of such lines to expected behavior. The extrapolation behavior of the functional form of this equation at low and high temperatures, pressures, and densities gives good confidence in the equation of state presented here in the absence of highly accurate experimental data over some areas of the fluid surface.

6. Summary

New thermodynamic data for dimethyl ether are presented over wide ranges of temperature and pressure. Vapor pressures were measured with a variable volume static apparatus from 265 K up to the visually detected critical point at 400.3 K. With an automated vibrating tube densimeter, densities of dimethyl ether were measured in the compressed liquid and supercritical states for temperatures from 273 to 523 K and pressures up to 40 MPa. The new vapor pressures, critical point, and compressed liquid densities were correlated with the TRIDEN model using the Tait, Rackett, and Wagner equations and compared with literature data. A new 10-parameter equation of state for dimethyl ether, valid from 131.65 to 525 K and for pressures up to 40 MPa, was fitted using the Helmholtz energy as the fundamental property. The equation of state is based on the experimental densities of dimethyl ether in the compressed liquid and supercritical states together with other published measurements from the literature. The uncertainty in density of the equation of state ranges from 0.1% in the liquid to 1% near the critical point. The uncertainty in heat capacities is 2%, and the uncertainty in vapor pressure is 0.25% at temperatures above 200 K. The uncertainty in vapor pressure increases at lower temperatures due to the lack of experimental data. In the critical region, the uncertainties are higher for all properties except vapor pressure. Although the

equation presented here is an interim equation, it represents the best currently available equation for the properties of DME.

List of symbols

a	Helmholtz energy
a^0	ideal gas Helmholtz energy
AAD	average absolute deviation
$A_R, \ldots, D_R$	parameters of Rackett equation
$A_W, \ldots, D_W$	parameters of Wagner equation
$B_T, \ldots, E_T$	parameters of Tait equation
c_p	heat capacity
P	pressure
P_0	reference pressure
P_c	critical pressure
R	universal gas constant (8.314472 J/(mol K))
T	temperature
T_c	critical temperature
T_r	reduced temperature (T/T_c)

Greek letters

α	dimensionless Helmholtz energy
α^0	dimensionless ideal gas Helmholtz energy
α^r	dimensionless residual Helmholtz energy
δ	reduced density (ρ/ρ_c)
ρ	density
ρ_c	critical density
τ	inverse reduced temperature (T_c/T)

References

[1] E.C. Ihmels, E.W. Lemmon, J. Gmehling, Fluid Phase Equilib. 207 (2003) 111–130.
[2] E.C. Ihmels, K. Fischer, J. Gmehling, Fluid Phase Equilib. 228/229 (2005) 155–171.
[3] E.W. Lemmon, E.C. Ihmels, Fluid Phase Equilib. 228/229 (2004) 173–187.
[4] R. Span, W. Wagner, E.W. Lemmon, R.T. Jacobsen, Fluid Phase Equilib. 183/184 (2001) 1–20.
[5] E.C. Ihmels, J. Gmehling, Ind. Eng. Chem. Res. 40 (2001) 4470–4477.
[6] E.C. Ihmels, Experimentelle Bestimmung, Korrelation und Vorhersage von Dichten und Dampfdrücken, Ph.D. Dissertation, University of Oldenburg, Shaker Verlag, Aachen, Germany, http://www.shaker.de, 2002.
[7] E.C. Ihmels, J. Gmehling, Int. J. Thermophys. 23 (2002) 709–743.
[8] E.C. Ihmels, S. Horstmann, K. Fischer, G. Scalabrin, J. Gmehling, Int. J. Thermophys. 23 (2002) 1571–1585.
[9] W. Wagner, A. Pruß, J. Phys. Chem. Ref. Data 31 (2002) 387–535.
[10] B.A. Younglove, J.F. Ely, J. Phys. Chem. Ref. Data 16 (1987) 577–798.
[11] D. Ambrose, J. Chem. Thermodyn. 18 (1986) 45–51.
[12] J. Wu, Z. Liu, B. Wang, J. Pan, J. Chem. Eng. Data 49 (2004) 704–708.
[13] A.C. Zawisza, S. Glowka, Bull. Acad. Pol. Sci., Ser. Sci. Chim. 18 (1970) 549–554.
[14] J.H. Dymond, R. Malhotra, Int. J. Thermophys. 9 (1988) 941–951.
[15] C.F. Spencer, R.P. Danner, J. Chem. Eng. Data 17 (1972) 236–241.
[16] S. Bobbo, M. Scattolini, L. Fedele, R. Camporese, V. De Stefani, J. Chem. Eng. Data 50 (2005) 1667–1671.
[17] Dortmund Data Bank for Pure Component Properties (DDB-Pure), DDBST GmbH, Oldenburg, Germany, http://www.ddbst.de, 2006.
[18] D.B. Pall, O. Maass, Can. J. Res. 14 (1936) 96–104.
[19] J. Wu, Z. Liu, F. Wang, C. Ren, J. Chem. Eng. Data 48 (2003) 1571–1573.
[20] O. Maass, E.H. Boomer, J. Am. Chem. Soc. 44 (1922) 1709–1730.
[21] J.C.G. Calado, L.P.N. Rebelo, W.B. Streett, J.A. Zollweg, J. Chem. Thermodyn. 18 (1986) 931–938.
[22] M. Frenkel, R.D. Chirico, V.V. Diky, X. Yan, Q. Dong, C. Muzny, NIST ThermoData Engine, Version 1.0. NIST Standard Reference Database 103, National Institute of Standards and Technology, Gaithersburg, MD, 2005. http://www.nist.gov/srd/nist103.htm.
[23] M. Frenkel, R.D. Chirico, V.V. Diky, X. Yan, Q. Dong, C. Muzny, J. Chem. Inform. Model. 45 (2005) 816–838.
[24] R. Span, W. Wagner, Int. J. Thermophys. 24 (2003) 1–39.
[25] E.W. Lemmon, R.T. Jacobsen, S.G. Penoncello, D.G. Friend, J. Phys. Chem. Ref. Data 29 (2000) 331–385.
[26] S. Bobbo, R. Camporese, R. Stryjek, J. Chem. Thermodyn. 30 (1998) 1041–1046.
[27] S. Bobbo, R. Camporese, R. Stryjek, S.K. Malanowski, J. Chem. Eng. Data 45 (2000) 829–832.
[28] S. Bobbo, L. Fedele, R. Camporese, R. Stryjek, Fluid Phase Equilib. 174 (2000) 3–12.
[29] S. Bobbo, L. Fedele, R. Camporese, R. Stryjek, Fluid Phase Equilib. 199 (2002) 153–160.
[30] S. Bobbo, L. Fedele, M. Scattolini, R. Camporese, R. Stryjek, Fluid Phase Equilib. 224 (2004) 119–123.
[31] E. Cardoso, A. Bruno, J. Chim. Phys. Phys.-Chim. Biol. 20 (1923) 347–351.
[32] E. Cardoso, A.A. Coppola, J. Chim. Phys. Phys.-Chim. Biol. 20 (1923) 337–346.
[33] E. Chang, J.C.G. Calado, W.B. Streett, J. Chem. Eng. Data 27 (1982) 293–298.
[34] J. Chao, K.R. Hall, Proc. Symp. Thermophys. Prop. 8 (1982) 71–77.
[35] H. Daiguji, E. Hihara, J. Chem. Eng. Data 48 (2003) 266–271.
[36] A. Eucken, E.U. Franck, Z. Elektrochem. Angew. Physik. Chem. 52 (1948) 195–204.
[37] L. Fedele, S. Bobbo, V. De Stefani, R. Camporese, R. Stryjek, J. Chem. Eng. Data 50 (2005) 128–132.
[38] L.J. Florusse, T. Fornari, S.B. Bottini, C.J. Peters, J. Supercrit. Fluids 22 (2002) 1–13.
[39] N.F. Giles, G.M. Wilson, J. Chem. Eng. Data 45 (2000) 146–153.
[40] A.V. Grosse, R.C. Wackher, C.B. Linn, J. Phys. Chem. 44 (1940) 275–296.
[41] H. Holldorff, H. Knapp, Fluid Phase Equilib. 40 (1988) 113–125.
[42] A. Jonasson, O. Persson, A. Fredenslund, J. Chem. Eng. Data 40 (1995) 296–300.
[43] R.M. Kennedy, M. Sagenkahn, J.G. Aston, J. Am. Chem. Soc. 63 (1941) 2267–2272.
[44] G.B. Kistiakowsky, W.W. Rice, J. Chem. Phys. 8 (1940) 222–618.
[45] T. Laursen, P. Rasmussen, S.I. Andersen, Can. J. Chem. 47 (2002) 198–202.
[46] T. Miyazaki, Proceedings of the 12th Japan Symposium on Thermphysical Properties, 1991, pp. 77–80.
[47] J.R. Noles, J.A. Zollweg, Fluid Phase Equilib. 66 (1991) 275–289.
[48] J.R. Noles, J.A. Zollweg, J. Chem. Eng. Data 37 (1992) 306–310.
[49] M.E. Pozo de Fernandez, J.C.G. Calado, J.A. Zollweg, W.B. Streett, Fluid Phase Equilib. 74 (1992) 289–302.
[50] Z. Seha, Chem. Listy 49 (1955) 1569–1570.
[51] M. Teodorescu, P. Rasmussen, J. Chem. Eng. Data 46 (2001) 640–646.
[52] C.Y. Tsang, W.B. Streett, J. Chem. Eng. Data 26 (1981) 155–159.
[53] T. Tsujimoto, H. Kubota, Y. Tanaka, S. Matsuo, T. Sotani, 13th Japan Symposium on Thermophysical Properties, 1992, pp. 217–220.
[54] A. Valtz, L. Gicquel, C. Coquelet, D. Richon, Fluid Phase Equilib. 230 (2005) 184–191.
[55] J. Wu, Z. Liu, J. Pan, X. Zhao, J. Chem. Eng. Data 49 (2004) 32–34.